bradscholars

Non-covalent adsorption of amino acid analogues on noble-metal nanoparticles: influence of edges and vertices

Item Type	Article
Authors	Hughes, Zak;Walsh, T.R.
Citation	Hughes ZE and Walsh TR (2016) Non-covalent adsorption of amino acid analogues on noble-metal nanoparticles: influence of edges and vertices. Physical Chemistry Chemical Physics. 18(26): 17525-17533.
DOI	https://doi.org/10.1039/C6CP02323A
Rights	(c) 2016 RSC. Full-text reproduced in accordance with the publisher's self-archiving policy.
Download date	2025-04-29 19:09:24
Link to Item	http://hdl.handle.net/10454/15841

Journal Name

ARTICLE

Non-covalent Adsorption of Amino Acid Analogues on Noble-metal Nanoparticles: Influence of Edges and Vertices

Z. E. Hughes[a] and T. R. Walsh[a,*]

The operation of many nanostructured biomolecular sensors and catalysts critically hinges on the manipulation of non-covalent adsorption of biomolecules at unfunctionalised noble-metal nanoparticles (NMNPs). Molecular-level structural details of the aqueous biomolecule/NMNP interface are pivotal to the successful realisation of these technologies, but such experimental data are currently scarce and challenging to obtain. Molecular simulations can generate these details, but are limited by the assumption of non-preferential adsorption to NMNP features. Here, via first principles calculations using a vdW-DF functional, and based on nanoscale sized NMNPs, we demonstrate that adsorption preferences to NP features varies with adsorbate chemistry. These results show a clear distinction between hydrocarbons, that prefer adsorption to facets over edges/vertices, over heteroatomic molecules that favour adsorption onto vertices over facets. Our data indicate the inability of widely-used force-fields like to correctly capture the adsorption of biomolecules onto NMNP surfaces under aqueous conditions. Our findings introduce a rational basis for the development of new force-fields that will reliably capture these phenomena.

Introduction

Facile molecular-level manipulation of the interface between biomolecules and nanomaterials in aqueous media promises transformative advances in a wide range of applications, including materials synthesis,[1-3] biosensing,[4,5] and nano-medicine.[6-8] Moreover, the ability to predictably manipulate the growth morphology of noble metal nanoparticles (NMNPs) in aqueous media via additive-based strategies, especially to produce non-spherical Au NP morphologies, is integral to exerting fine control over NP size and shape.[9-15] Knowing how and where these additives prefer to bind at the NP interface is key to realizing these strategies[16].

NMNPs are of particular interest since they possess both desirable optical and plasmonic properties,[7,17,18] and as reported recently, peptide-enabled catalytic properties.[13, 15,19,20] However, by definition, most bio-related NMNP applications are realised under aqueous conditions, where the NMNPs must be passivated by molecules to prevent uncontrolled NP aggregation in solution.

[a.] Institute for Frontier Materials, Deakin University, Geelong VIC 3216, Australia.
Fax: +61 (0)3 5227 1103; Tel: +61 (0)3 5227 3116;
E-mail: tiffany.walsh@deakin.edu.au

Electronic Supplementary Information (ESI) available: Structural details of the bare NMNPs; locations of the different sites on the NP surface; detailed site adsorption energies of water, methane and benzene; adsorbate-surface distances for optimised geometries; plots correlating adsorption energies on Pt$_{147}$; minimum energy configurations of water, methane and benzene at the different sites on Au$_{147}$; isosurface plots of bonding orbitals of methanamine adsorbed on Au$_{147}$; averaged interfacial water density for Au$_{147}$ in liquid water from molecular dynamics simulations; comparison of NP facet vs. infinite planar surfaces for adsorbates adsorbed on Au and Pt; comparison of adsorption energies with different cutoffs. See DOI: 10.1039/x0xx00000x

Traditionally this has been accomplished using covalently-attached ligands (such as thiol-based ligands on Au NPs). However, non-covalent NMNP passivation is known to be effective; for example, citrate is a widely-used agent for both Au NP growth and dispersion in aqueous media,[21] which can be non-covalently exchanged for other ligands.[22] Recent exploitation of non-covalent metal-biomolecule interactions in this area has included the use of peptides as agents to realise the in-situ nucleation, growth, dispersion, and catalytic activation of NMNPs in aqueous solution.[9–15] Moreover, the direct non-covalent adsorption of nucleic acid aptamers onto unfunctionalised NMNPs is a key component of successful biomolecular sensor design (see Martin et al.[5] for a recent example).

A fundamental knowledge base, in the form of molecular-level structural data of these biomolecule-decorated NMNPs, is required to fully exploit the emergent properties from these novel and versatile systems. Availability of such data is currently limited. Circular dichroism (CD) spectroscopy can broadly indicate the presence of secondary-structural motifs, but such motifs are often absent for the size range of peptide sequences used in these applications.[15] Nuclear magnetic resonance (NMR) spectroscopy can, in principle, provide these insights,[23] but in practice can be limited in its applicability to these systems. As a consequence, much of the published structural data for peptide– nanoparticle interfaces has been generated via molecular dynamics (MD) simulations. MD simulations can provide the required level of structural resolution, but can be limited by a lack of reliability, particularly because it is challenging to verify the interatomic potentials (herein referred to as force-fields, FFs) that are used to describe the interactions at the biomolecule–NP interface. Many of the key points of FF verification must be sourced from the very same experimental structural data

that are so challenging to obtain in the first instance, thus impeding the advancement of reliable force-fields suitable for use in describing bio/NP interfaces.

This limitation notwithstanding, a number of recent studies have reported the application of MD simulation to the investigation of interactions of biomolecules with aqueous noble metal interfaces.[13,24–34] However, the majority of these studies modelled the adsorption of peptides at periodic planar interfaces as an approximation to the NMNP surface. Even in those instances when the adsorption to stepped noble metal surfaces or actual NMNP surfaces was investigated, the FFs employed in these studies were designed for use with infinite planar surfaces without the presence of low-coordinated metal atom sites.[11,27,35] Moreover, while these studies might have been capable of capturing the influence on peptide adsorption of the presence of finite facets on the NP, it is unlikely that a FF designed to describe facet adsorption alone can appropriately capture and distinguish the preferences of biomolecular adsorption to NP features such as edges and vertices. Specifically, the metal atoms in such FFs all adsorb with the same 'in-plane' propensities, regardless of whether each atom is situated at a facet, edge or vertex. Therefore, based on our earlier successful first-principles (FP) calculations of biomolecule adsorption onto noble metal planar surfaces,[36–38] here we have used FP density functional theory calculations to predict the preferential adsorption of biomolecules on NMNP surface features.

FP calculations have been extensively used to investigate a range of attributes for noble metal surfaces and NPs. Previously, FP calculations have been used to study the shape and structure of NMNPs[39–45] as well as the covalent attachment of ligands to NMNP surfaces.[19,20,46–55] The use of FP calculations to investigate the non-covalent adsorption of molecules to NMNPs has not been as extensively reported.[51,56–58] Of these few earlier studies, all used standard generalised-gradient approximation (GGA) density

functionals, which are known to perform extremely poorly in such weakly-bound cases,[59,60] and were based on much smaller (sub-nanometer) NP sizes. Moreover, none of these studies focused on differences in adsorption depending on NP site.

Our calculations differ from many previously-reported FP studies of both covalent and non-covalent adsorption on NMNPs[20,46–51,53–57,61–63] in two key aspects. First, we considered nanometer-sized Au_{147} and Pt_{147} cubooctahedral nanoparticles in our FP calculations, with vertex-to-vertex dimensions of 1.72 nm and 1.66 nm respectively, where most previous studies considered much smaller nanoclusters. One very recent exception to this is a study of covalent adsorption of mono- and diatomic species reported by Peng and Mavrikakis[58] who also considered the Pt_{147} NP. The size of our nanoparticles is relevant to very recent studies, where peptides have been used as in-situ growth and capping agents to disperse NMNPs in aqueous solution, producing stable dispersions of NPs with a diameter of ~2.5 nm.[12,15,32]

Second, we have used a vdW-DF functional, namely the revPBE-vdW-DF [64] functional. The vdW-DF family of functionals incorporates a non-local form of the correlation functional and is not based on empirical post-hoc corrections. [60] These functionals significantly improve the performance of density functional theory in capturing the non-covalent contribution to the interaction energy at medium- to long-range inter-atomic separations.[65] vdW-DF functionals are gaining wider use in the determination of *in vacuo* adsorption energies and structures of molecules noncovalently adsorbed on noble-metal surfaces in the case of infinite planar surfaces.[36–38,66–71] We have previously used plane wave density functional theory (PW-DFT) with vdW-DF functionals to calculate adsorption energies of biomolecules to infinite planar Au(111), Au(100)(1×1) and Au(100)(5×1) surfaces.[36,37] These calculations were all performed using the revPBE-vdW-DF[64] functional; comparison of our calculated adsorption energies of molecules, mostly alkanes of varying size, to the Au(111) surface calculated via revPBEvdW-DF with those determined from experiment showed outstanding agreement.[36]

Here, we have rigorously investigated and determined the non-covalent adsorption energies and minimum energy configurations of a variety of different small organic molecules containing the same functional groups present in the side-chains of amino acids, as well as water, to various sites (facets, edges and vertices) located on cubooctahedral Au_{147} and Pt_{147}, using PW-DFT calculations with the revPBE-vdW-DF functional. Our set of adsorbates covers a range of amino acid physicochemical properties including non-polar molecules, polar molecules and aromatic molecules.

Methodology

The set of nine adsorbate molecules considered here (see Table 1) was chosen to span the range of the functional groups found in amino acids. To obtain these configurations, we fully relaxed all atoms in these systems using geometry optimisation, using a large range of initial geometries and adsorption sites, as described herein. A full and detailed description of the set of adsorption sites is provided in Figs S1 and S2 of the ESI.
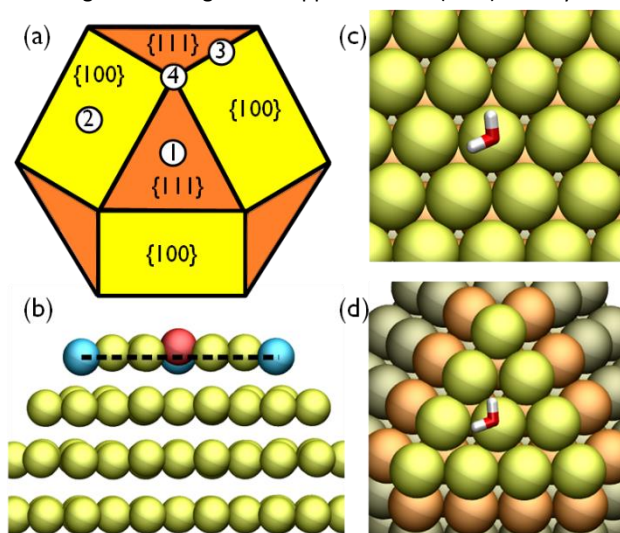

Figure 1. (a) Schematic of the NM_{147} cubooctahedral NP. The numbered circles indicate the general location of the four main sites, 1={111} facet, 2={100} facet, 3=edge and 4=vertex. **(b)** Buckling of the {111} facet on the Au_{147} NP; blue and red spheres indicate the corner and facet-center atoms respectively. The dashed line indicates the average position of the atoms in the facet plane. Minimum energy configurations of water on **(c)** the periodic (111) surface and **(d)** {111} facet of the NP; gold atoms are colored differently to better enable identification of sites.

To identify equilibrium adsorption geometries and subsequently calculate adsorption their corresponding adsorption energies on the NM$_{147}$ NP (either Au$_{147}$ or Pt$_{147}$), we followed the process reported previously to calculate the adsorption energy of small molecules on infinite planar metal surfaces.[36–38] Initially, each molecule was positioned close to the NP surface and the geometry was optimised with all atoms in both the adsorbate and the NP allowed to relax. We explored a wide range of adsorbate/surface configurations in each case. Moreover, we have previously investigated a number of different adsorbed configurations for the same molecules adsorbed at the infinite planar Au(111) and Au(100) surfaces[36] and we used the minimum energy configurations that resulted from these calculations as the basis of some of the initial adsorption geometries used here. After each geometry had been optimised, the adsorption energy of the system was then determined from a single-point energy calculation. The adsorption energy, E_{ads}, was calculated using

$$E_{ads} = E_{NP\text{-}mol} - E_{NP} - E_{mol} \qquad (1)$$

where $E_{NP\text{-}mol}$ is the energy of the system with the molecule adsorbed to the NMNP surface, E_{NP} is the energy of the NMNP, and E_{mol} is the energy of the molecule in vacuum.

All PW-DFT calculations were performed with the Quantum Espresso code, versions 5.0.5.[72] The revPBE-vdW-DF exchange-correlation functional[64,73] and ultrasoft pseudopotentials[74] were used to calculate the adsorption energies. All calculations were performed using cutoffs for the plane-wave kinetic energy and electron densities of 25 and 250 Ry, respectively, and were not spin-polarised. In selected cases, longer cutoffs were used (as indicated in the Results). The Gaussian smearing method, with a width of 0.05 Ry, was used for Brillouin zone integration. The SCF calculation convergence threshold was set to 1×10^{-6} Ry for all calculations. For the geometry optimisations a 0.026 eV/Å force convergence criterion was applied; during the single point calculations the forces were checked to ensure the threshold was not exceeded. These cutoffs (and the convergence criteria) are the same as those previously used for the infinite planar calculations.[36,37]

All calculations used periodic boundary conditions applied in all three dimensions. For the geometry optimisations, the NP was placed in the centre of a 29.1×29.1×29.1 Å^3 cell, providing a minimum separation distance between the NP and its periodic image of ~12 Å, again consistent with the infinite planar calculations. For the single-point energy calculations, the cell size was increased to 39.7×39.7×39.7 Å^3, providing a minimum separation distance of ~22.5 Å, (with corresponding infinite planar calculations having a separation of ~25 Å). All such calculations were performed at the gamma point.

In addition to the calculations outlined above, geometry optimisations of the bare NPs were also performed using a variety of traditional functionals, namely PBE[75], revPBE[73] and PBEsol[76], in addition to the revPBE-vdW-DF functional, to investigate the buckling of the NP facets (*vide infra*).

The adsorption energies for some of our adsorbates to the infinite planar Au(111) and Au(100) surfaces had not been reported

Table 1: Adsorption energies, E$_{ads}$, of adsorbates on Au$_{147}$ and Pt$_{147}$. The most and least favorable sites are highlighted in bold font and underlined, respectively.

Adsorbate	Metal	E_{ads} [kJ mol^{-1}]			
		{111}	{100}	Edge	Vertex
Methane	Au	-11.9	**-13.9**	-10.1	<u>-7.7</u>
	Pt	-12.8	**-15.2**	-11.0	<u>-9.2</u>
Ethane	Au	-17.8	**-20.4**	-15.8	<u>-11.0</u>
	Pt	-18.9	**-22.2**	-17.1	<u>-16.4</u>
Benzene	Au	-39.2	**-48.1**	-40.8	<u>-38.7</u>
	Pt	<u>-48.0</u>	**-112.2**	-99.6	-84.8
Water	Au	<u>-15.6</u>	-19.0	-17.7	**-20.8**
	Pt	<u>-19.8</u>	-26.3	-28.3	**-38.7**
Methanol	Au	<u>-25.3</u>	-29.5	-26.7	**-30.9**
	Pt	<u>-32.1</u>	-40.6	-41.6	**-54.6**
Methanamide	Au	<u>-31.3</u>	-38.6	-35.7	**-46.1**
	Pt	<u>-43.1</u>	-59.7	-60.8	**-73.7**
Methanamine	Au	<u>-53.1</u>	-64.2	-61.8	**-72.7**
	Pt	<u>-86.4</u>	-102.4	-102.3	**-119.7**
Imidazole	Au	<u>-55.7</u>	-66.9	-65.4	**-79.8**
	Pt	<u>-91.4</u>	-107.8	-109.1	**-132.5**
Dimethyl sulfide	Au	<u>-59.3</u>	-71.1	-71.4	**-80.9**
	Pt	<u>-103.3</u>	-124.3	-124.8	**-139.3**

previously; for these molecules/surfaces the adsorption energies were calculated on the infinite planar surface consistent with methodology outlined above and in our previous studies.[36,37]

Results and discussion

We start with our geometry-optimised structures of the bare NM$_{147}$ cuboctahedral Au and Pt NPs. These NPs possess both {111} and {100} facets, shown in Fig. 1a). The minimum energy structure of the bare NPs differed from the structure of the ideal truncate of the bulk crystal, in that the facets were not perfectly planar. We found that both the {111} and {100} facets of both NPs buckled such that they protruded slightly, Fig. 1(b), with the atoms at the facet centre located farthest from the plane, as defined by the positions of the facet corners. The calculated maximum displacement of atoms relative to this plane was 0.45 Å and 0.38 Å for the {111} and {100} facets respectively for Au$_{147}$. Similar behaviour to a lesser degree was noted for Pt$_{147}$, with maximum out-of-plane displacements of 0.25 Å and 0.21 Å for the {111} and {100} facets respectively.
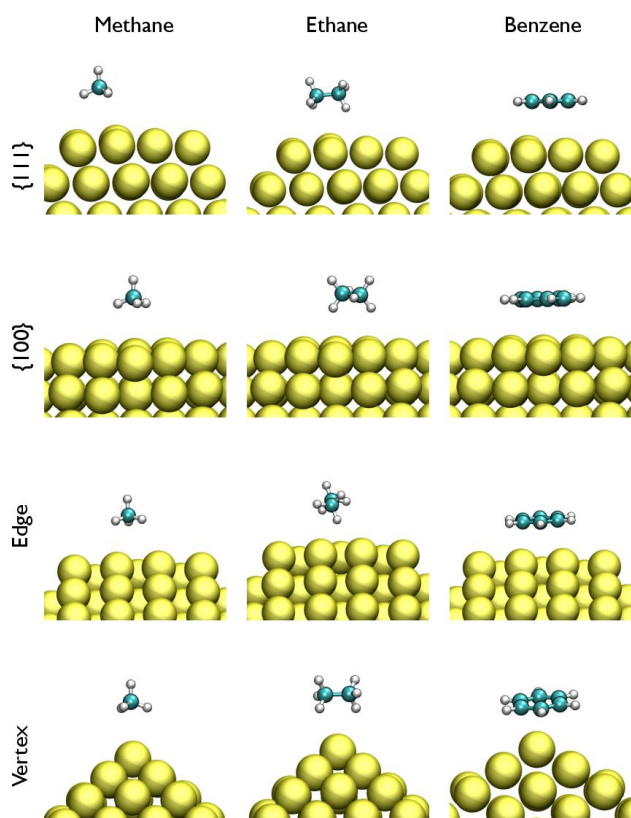
Figure 2: Optimal adsorption geometries for each type of site (facet, edge and vertex) on Au_{147}, for methane, ethane and benzene.

For Au_{147} we also investigated this effect using a range of PBE-based, traditional density functionals; PBE,[75] revPBE[73] and PBEsol.[76] All functionals supported facet buckling with varying degrees of displacements (see Table S1, ESI). All of these calculations were performed at the gamma-point. We also calculated the inter-planar spacings along both the <111> and <100> directions of the Au_{147} NP (see Table S2, ESI). Our previous experience in recovering the experimentally-determined structures of in-plane buckling of Au(100)(5 × 1) surfaces using revPBEvdW-DF calculations[37] supports our approach here; however, we suggest that our predicted buckling amplitudes most likely represent an upper bound.

Next, we calculated the optimised geometries and their corresponding non-covalent adsorption energies of nine adsorbates to Au_{147} and Pt_{147} at the {111}, {100}, edge and vertex sites, summarised in Table 1. The optimal adsorption geometries for Au_{147} are provided in Figs 2-4, while the corresponding geometries for Pt_{147} were very similar, except for benzene (*vide infra*). Relevant adsorbate—surface distances are given in Table S3 of the ESI for both Au_{147} and Pt_{147}. A detailed breakdown of the adsorption energies at the fourteen different NP sites for water, methane and benzene is provided in the ESI, Tables S4-S6, with illustration of all corresponding detailed sites present on the NP surface given in Figs S1 and S2 of the ESI. In Table 1 we highlighted the strongest and weakest binding site for each adsorbate. These data reveal two clear categories of adsorbates; the hydrocarbons, that favour adsorption to the NP facets, and the heteroatomic molecules (including water) that exhibit binding preference to NP vertices. We

also summarise these findings graphically in Fig. 5a) for Au_{147} and Fig. S3, ESI for Pt_{147}.

The aliphatic hydrocarbon adsorbates followed the same general ranking of binding site preferences, regardless of noble-metal type, with {100} > {111} > edge > vertex. Optimal adsorption geometries for methane and benzene, at all the sites tested, are presented in Figs S4 and S5 of the ESI. Taken together, these aliphatic hydrocarbon binding preferences, along with their increase in binding strength with adsorbate size (in terms of binding surface area), are entirely consistent with van der Waals (vdW)-dominated molecule-surface interactions. However, the adsorption of benzene, our exemplar aromatic hydrocarbon adsorbate, could not be so simply categorised across both metal NPs (see below).

In the case of Au_{147}, the adsorption of benzene followed the same trend as the aliphatic hydrocarbons, where the {100} facet was the preferred binding site and the vertex site was the least favourable. However, this trend did not hold for Pt_{147}. Although benzene adsorbed most strongly on the {100} facet of Pt_{147}, we found that the least favourable binding location was the {111} facet, and not the vertex site. We propose that this anomalous adsorption trend for benzene adsorbed on Pt_{147} arises from two main factors. First, because benzene has the greatest spatial extent of all the adsorbates tested, we suggest that the edge-effects of the NMNPs are at their most apparent for benzene. In addition, the surface area of the {111} facet is smaller than that of the {100}; on Pt_{147} the areas are 30.2 $Å^2$ and 69.2 $Å^2$, respectively. This means that these edge effects may be more noticeable in the case of the {111} facet than the {100} facet. These edge effects are apparent in Fig 5b)
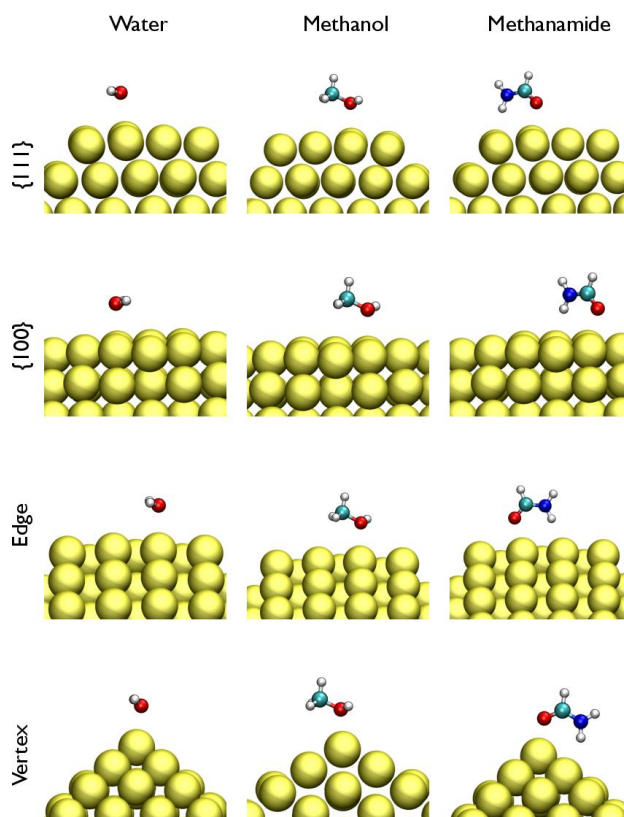

Figure 3: Optimal adsorption geometries for each type of site (facet, edge and vertex) on Au_{147}, for water, methanol and methanamide.

where the adsorption energies of the adsorbates to the {111} and {100} facets of Au_{147} are plotted against the corresponding adsorption energies at the infinite planar surfaces. Of all the
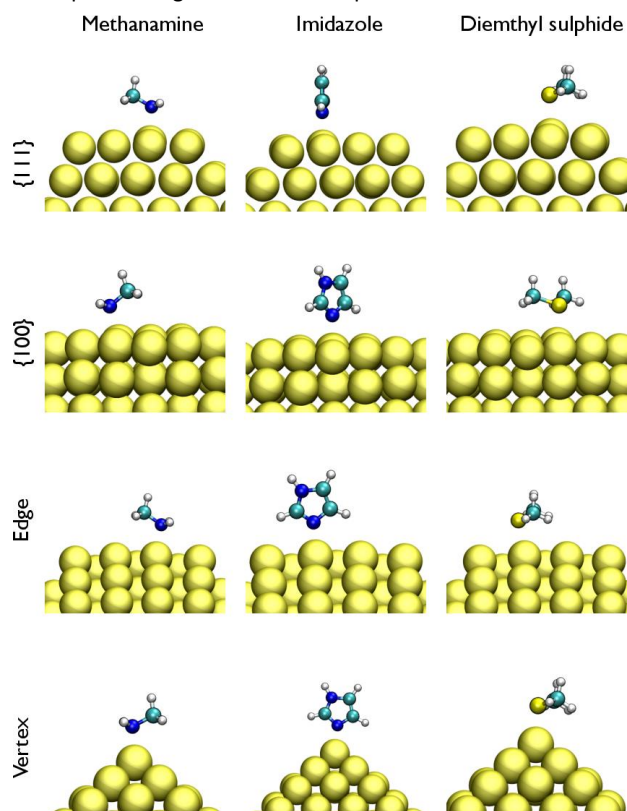

Figure 4: Optimal adsorption geometries for each type of site (facet, edge and vertex) on Au_{147}, for methanamine, imidazole and dimethyl sulphide.

molecules tested, benzene showed the greatest discrepancy; furthermore the difference is greater for the {111} facet than the {100} facet. This finding is underscored by available experimental data for the adsorption of benzene on both the Au(111) and Pt(111) planar surfaces (see Tables S7 and S8).

Second, the adsorbed geometry of benzene on the {100} facet, and the corresponding interactions governing this adsorption, revealed distinct differences between the two noble metals. As noted for the aliphatic hydrocarbons, a vdW-dominated interaction is suggested for benzene adsorbed on the Au_{147} {111} and {100} facets, as indicated by isosurfaces of bonding orbitals shown in Fig. 6a). In this image benzene is shown to adsorb in a flat orientation on the {100} facet, with a lack of electronic coupling suggested between the adsorbate and NP. For Pt_{147} the binding is more complex; while benzene also adsorbed in a planar configuration on the {111} facet, for the {100} facet the molecule adsorbed in a buckled configuration with the hydrogens pushed out of plane (Fig. 6b)). Taken together, the adsorption of benzene to the {100} facet of Pt_{147} appears to support a greater degree of weak chemisorption character compared with benzene adsorbed at the {111} facet of Pt_{147}.[66-68] In Fig. 6b), isosurfaces of relevant bonding orbitals indicate electronic coupling between the Pt_{147} and benzene that were not present for Au_{147}.

All of the heteroatomic adsorbates supported the following trend in adsorption strength across both NMNPs, with vertex >

edge ≈ {100} > {111}. The optimised adsorption geometries of water on the detailed sites on Au_{147} are shown in Figs S6 and S7 of the ESI. Our predicted ranking in binding site preference is inconsistent with a vdW-driven mode of adsorption. This finding is significant because a vdW-driven mode of adsorption has been assumed by all current NMNP/biomolecule/water force-fields used to describe molecular simulations of non-covalent interactions between biomolecules and NMNPs;[11,27,35] our results suggest these assumption is incorrect.

We also checked that the ranking of adsorption site preferences for both heteroatomic and hydrocarbon adsorbates was robust to the choice of the cutoffs used in our DFT calculations. To do this, we re-calculated the adsorption energies of methane and water at the {111} and {100} facets, edges and vertices of Au_{147} using two sets of higher cutoffs; 35 (280) Ry and 50 (400) Ry for the plane wave kinetic energy (electron densities). These binding energy data are summarised in Table S9 of the ESI, and indicate that our choice of cutoffs is sufficient here.
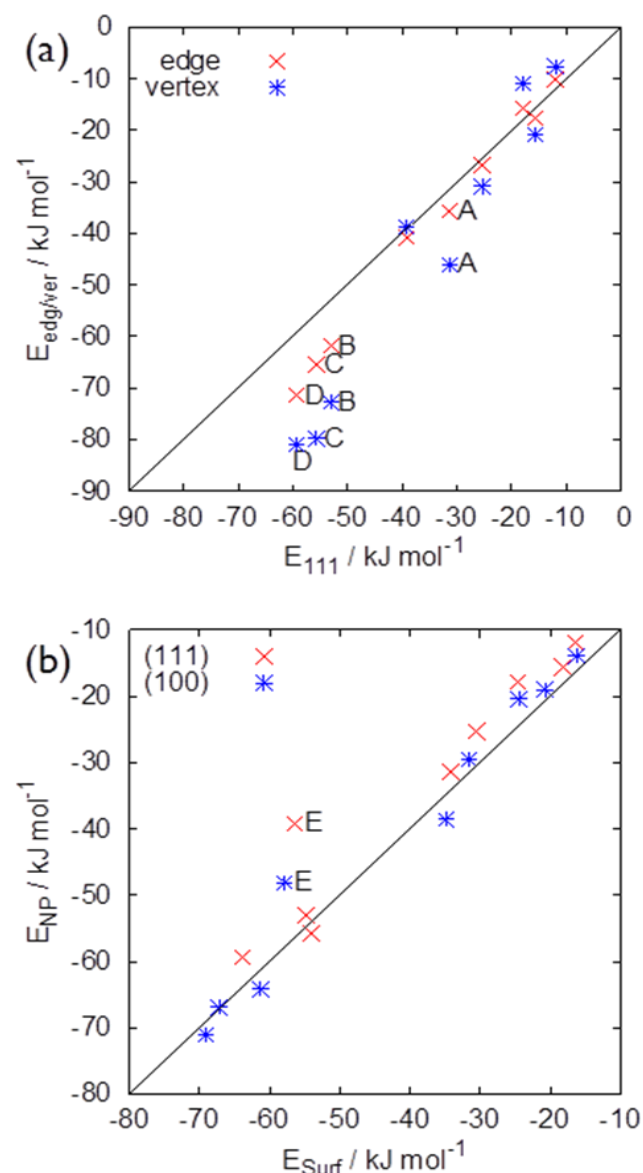

Figure 5. Comparison of adsorption energies for (a) the {111} facet against the edge and vertex sites of Au_{147}, and (b) the Au_{147} facets against their counterpart infinite planar surfaces. Labels for the different molecules indicate: A-methanamide, B-methanamine, C-imidazole and D-dimethyl sulphide, E-benzene.

All of the heteroatomic adsorbates considered here have previously been described as 'weakly chemisorbing' to Au(111) and Au(100) infinite planar surfaces,[36,37,77] with the interaction being mediated chiefly via the heteroatom (*e.g.* N, O or S). We propose that this weak chemisorption drives the strong preference for the vertex site in these cases.[52] Example isosurfaces of relevant bonding orbitals for methanamine adsorbed on both the {111} facet and the vertex site of Au_{147} are provided in Fig. S8 of the ESI, suggesting electronic coupling between the NP and adsorbate. The difference in adsorption strength between the vertex and the {111} facet is substantial for methanamine, imidazole and dimethyl sulphide, which favoured the vertex by 19.6 (33.3), 24.1 (41.1) and 21.6 (36.0) kJ mol^{-1}, respectively, for Au_{147} (Pt_{147}). It is noted that these differences are much greater than the corresponding adsorption energy differences between the infinite planar Au(111) and Au(100) surfaces. This finding is also significant, because our previous studies have shown that these small energy differences calculated for *in-vacuo* adsorption on the two surface planes actually translated into substantial differences in the adsorption of biomolecules to the (111) and (100) Au surfaces.[34,37]

The adsorption preferences of water are of particular interest. The interfacial structuring of liquid water at inorganic material

Figure 6. Isosurfaces of representative bonding orbitals for benzene adsorbed on the {100} facet of **(a)** Au_{147} and **(b)** Pt_{147}. The isosurfaces are shown for 1×10^{-5} e/Å^3.

interfaces is thought to exert substantive influence of adsorption behaviour of biomolecules at such surfaces. This has been reported not only in the cases of strongly hydrophilic interfaces such as titania and silica[78,79] but also for noble metals,[28–30,34,36–38] including very recent elucidation of the role of interfacial water in facet-selective peptide adsorption at different aqueous Au planes.[34] On the basis of these previous studies, we predict that the differences in binding-site preferences noted here will confer a highly non-uniform spatial distribution of interfacial solvent structuring around the NMNP. Specifically, our findings suggest that a higher density of interfacial water at the NP vertices and edges, and a relatively lower density at the facets, is likely. As we shall show herein, this structuring is not recovered by current NMNP/water inter-atomic potentials. This potentially incorrect description of solvent structuring at the NMNP/water interface could provide misleading predictions of adsorption site preferences of biomolecules under aqueous conditions.

To underscore this hypothesis, we performed two types of test using a force-field that has been previously used to model biomolecule adsorption to faceted aqueous NMNPs,[11,27,35] CHARMM-METAL,[80] to probe the interaction between our Au_{147} NP and water. In the first test, we investigated the *in-vacuo* adsorption of a single water molecule on the Au_{147} NP using CHARMM-METAL. Using this force-field, we found that the water molecule overwhelmingly favoured the facet adsorption site with a binding energy of -19.0 kJ mol^{-1}. At first glance, this particular adsorption energy value agrees well with our vdW-DF calculations for the facet site. This agreement makes sense, because the CHARMM-METAL force-field was originally designed for use with noble metal *planes*. However, we could not locate *any* stable geometries corresponding with adsorption at the vertex site using CHARMM-METAL. Only by performing a series of single-point energy calculations (*i.e.* not letting any atomic positions relax), as a function of fixed distance between the water oxygen atom from the vertex Au atom, could we identify a lowest possible CHARMM-METAL binding energy of -7.6 kJ mol^{-1} at the vertex site. We emphasise here that this is not an equilibrium binding energy, because the structure corresponding to this energy is not stable with respect to geometry optimisation. This CHARMM-METAL trend directly contradicts our vdW-DF results, and we expect this to be the case for most such heteroatomic adsorbates.

In our second test, we performed molecular dynamics simulations of our Au_{147} NP in liquid water using the CHARMM-METAL model. The averaged interfacial water density around the NP, shown in Fig. S9 of the ESI, revealed that water structuring around the NP vertices and edges was weaker compared with the structuring at the NP facets. This is not a criticism of CHARMM-METAL as applied to infinite planes; our findings for Au NP solvation quite reasonably reflect the fact that CHARMM-METAL was originally designed to capture adsorption to infinite planar metal surfaces. However, the application of any force-field to systems for which it was not designed is an established caveat of molecular simulation in general. Therefore, we recommend that data generated from simulations of the interface between water, biomolecules and faceted NPs that have used such force-fields should be cautiously interpreted with this caveat in mind.
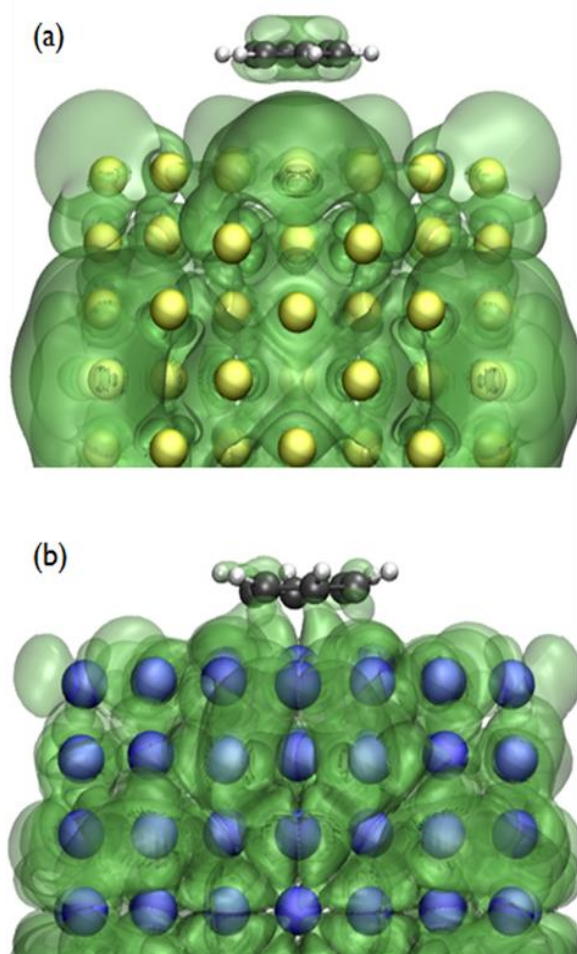
In addition to exploring NP feature-selective adsorption, we also compared the differences in adsorption energies at the {111} and {100} Au$_{147}$ facets with their counterpart energies obtained for infinite planar surfaces of Au(111) and Au(100).[36,38] For all adsorbates these data are summarised graphically in Fig. 5b), with absolute values provided in Table S7 in the ESI. With four exceptions (out of eighteen data points), adsorption was broadly found to be weaker at the Au$_{147}$ {111} and {100} facets relative to their infinite planar counterparts. These exceptions aside (see below), we suggest that this relative weakness of facet adsorption on the NP surface compared with the infinite planar surface may be due to the absence of delocalised metallic electronic states (corresponding to the metallic state of the infinite planar surface) in the NP. While studies have indicated that *covalent* bonding energies of adsorbates on Au NPs facets can be *stronger* than that corresponding to infinite planar surfaces, due to the discretisation of the orbital spacings near the HOMO level,[62] there is no evidence to indicate that such factors must influence non-covalent adsorption energies in a similar manner.

All four counter-examples in this comparison were heteroatomic adsorbates; this set comprised imidazole adsorbed on Au {111}, and methanamide, methanamine and dimethyl sulphide adsorbed on Au {100}. We suggest that the stronger adsorption of these molecules on the NP facet compared with the infinite planar counterpart surface could be due to the weakly-chemisorbing nature of these adsorbates. These four molecules exhibited the greatest feature-selective binding energy differences on Au$_{147}$, see Fig. 5a). One additional factor that may also play a role is that the NP facet surfaces were slightly outwardly buckled rather than strictly planar. Because the infinite planar surfaces will represent an upper limit on the facet binding energies, we expect that the facet-selective binding trends reported here will hold for larger NP sizes.

We explored the comparison of adsorption on the NP facet *vs.* infinite planar surface in detail for water adsorption (Table S4, ESI), and found adsorption to be weaker at the Au$_{147}$ {111} and {100} facets relative to their infinite planar counterparts. However, as previously reported for the infinite planar surfaces, atop sites remained the preferred site on both types of NP facet. The optimised adsorbed configurations were effectively unchanged from those found for the infinite planar surfaces, as shown in Figs 1(c) and (d), and Figs S6 and S7 of the ESI. The oxygen atom of the water molecule was located atop the Au atom with the molecule oriented such that the dipole was slightly tilted with respect to the plane of the facet.

Furthermore, we also sought to make comparisons with experimental binding energy data, where available, as summarized in Tables S7 and S8 of the ESI for Au and Pt respectively. As concluded from recent previous studies and review articles,[81-82] accurate experimental measurements of non-covalent adsorption energies for small molecules (other than diatomics such as CO and H$_2$, *etc*) adsorbed on *planar* Au and Pt surfaces are remarkably lacking yet much needed. This challenge is particularly acute for polar adsorbates such as water and methanol, where adsorbate clustering is known to occur on these metal surfaces, even at very low coverages.[83-85] The resulting interplay between adsorption energy and spatial distribution of these adsorbates (often lacking long-ranged ordering, especially in the case of Pt) leads to a substantial increase in the apparent surface-binding energy.[85] Due to these caveats, we maintain that comparisons with available experimental adsorption data for water and methanol are not meaningful in this instance. Experimental binding energy data for Au nanoparticles (as opposed to small Au clusters) is even more limited; in Table S7 we report binding energy data taken from experiments that considered Au nanoparticles on alumina or silica supports – and again, caveats apply to this comparison, given that the nature of the support may influence the adsorption energy. In addition, we could not find any such data for Pt nanoparticles (as opposed to small Pt clusters).

Nonetheless, for methane, ethane and benzene, we find that our calculations on Au$_{147}$ and the planar Au surface agree favourably with the experimental data (Table S7), given that we predict adsorption to be less strong on the NP facet compared with the corresponding planar surface. These data also reinforce our arguments articulated earlier regarding the fact that the size of the {111} facet on NMNP$_{147}$ is small compared with the spatial extent of benzene (leading to a substantial difference between the facet and planar adsorption energies in this case). For the case of Pt (Table S8), both methane and ethane agree well with the experimental values, given that we expect the NP adsorption to be weaker than that on the corresponding planar surface. While there are no reliable experimental data for adsorption of water (in monomer form), the trend between the previously-reported binding energy on planar Pt(111)[82] and our calculated binding energy on the Pt{111} facet is similarly consistent. Benzene is the only adsorbate for which data were available for both DFT (revPBE-vdW-DF) binding energies on Pt$_{147}${111} facet and the planar Pt(111) surface, and experimental binding energies on the Pt(111) surface. In this case, while the previously reported DFT calculations[68,86] of the planar Pt(111) binding energy are clearly weaker than those reported from experiment, our Pt$_{147}${111} facet adsorption energy is consistently weaker with these previously-reported DFT data (see arguments above regarding the size of the Pt{111} facet).

While it is reasonable to infer from our results that the adsorption of biomolecules at the aqueous NMNP interface will show feature-selective preferences, we are cautious to extrapolate from our results to directly and precisely predict the spatial patterning of adsorption behaviour arising from biomolecules interacting with NMNPs in liquid water. This is due to the complex interplay between the degree of interfacial water structuring and the underlying binding enthalpy of the adsorbate. Consider, for example, the more favourable adsorption of molecules to the (100) surface than to the (111) surface of Au and Ag *in vacuo*.[36–38] Naively, this may suggest this difference would translate into *stronger* adsorption of biomolecules at the aqueous Au/Ag (100) interface. On the contrary, detailed simulations instead revealed that the greater structuring of interfacial liquid water at the (100) interface confers the opposite effect,[87] with most amino acids and peptides adsorbing more strongly to the aqueous Au(111) interface.[36,37] Nonetheless, under aqueous conditions we generally expect that residues with heteroatomic side-chains such as Met, His and Lys may still prefer adsorption to vertex sites over facets, while

hydrophobic residues might find the NP facets to be a more favourable adsorption location.

The inability of current bio/NP force-fields to recover the feature-selective preferences revealed here raises serious challenges for molecular simulations that are aimed at predicting this chemical and spatial NP surface patterning under aqueous conditions. Our results provide the essential foundations for development of a model to enable this, which, by definition, will need to exceed the complexity of the vdW-based force-fields currently available. To capture weak chemisorption effects, bespoke non-bonded pairwise interactions (*e.g.* Lennard-Jones interactions), as has been successfully implemented for more sophisticated force-fields for infinite planar Au surfaces,[36,37,77] should be incorporated. Moreover, these alone may not be sufficient to ensure vertex- and edge-selective adsorption; we suggest that additional use of virtual sites, as used for planar Au surfaces[36,37,77] may be usefully employed around edges and vertices to ensure correct adsorption geometries.

Conclusions

In summary, we have used first principles calculations, applied to nanoscale-sized noble-metal nanoparticles, to reveal the variation in preferential adsorption of different adsorbate chemistries across all sites of the nanoparticle. Our findings reveal clear preferences for heteroatomic adsorbates to favour vertices and edges over facets, while conversely hydrocarbons are more strongly bound at facets than edges or vertices. These variations in preferred binding site cannot be recovered by current force-fields used to describe the aqueous bio/nanoparticle interface. The consequences of this predicted spatial and chemical variation in preferred binding site are explored in terms of the implications for future simulations of biomolecule adsorption to faceted noble metal nanoparticles under aqueous conditions. Our results provide the foundations for a genuinely feature-selective force-field for reliably describing the aqueous biotic/abiotic nanointerface.

Acknowledgements

References

1   R. R. Naik, S. J. Stringer, G. Agarwal, S. E. Jones and M. O. Stone, *Nat. Mater.*, 2002, **1**, 169–172.
2   M. Hnilova, C. R. So, E. E. Oren, B. R. Wilson, T. Kacar, C. Tamerler and M. Sarikaya, *Soft Matter*, 2012, **8**, 4327–4334.
3   S. V. Patwardhan, F. S. Emami, R. J. Berry, S. E. Jones, R. R. Naik, O. Deschaume, H. Heinz and C. C. Perry, *J. Am. Chem. Soc.*, 2012, **134**, 6244–6256.
4   R. Baron, B. Willner and I. Willner, *Chem. Comm.*, 2007, 323–332.
5   J. A. Martin, J. L. Chavez, Y. Chusak, R. R. Chapleau, J. Hagen and K.-L. N, *Anal. Bioanal. Chem.*, 2014, **406**, 4637–4647.
6   M. Chakraborty, S. Jain and V. Rani, *Appl. Biochem. Biotech.*, 2011, **165**, 1178–1187.
7   J. A. Webb and R. Bardhan, *Nanoscale*, 2014, **6**, 2502.
8   Y. Xia, W. Li, C. M. Cobley, J. Chen, X. Xia, Q. Zhang, M. Yang, E. C. Cho and P. K. Brown, *Acc. Chem. Res.*, 2011, **44**, 914–924.
9   L. M. Forbes, A. P. Goodwin and J. N. Cha, *Chem. Mater.*, 2010, **22**, 6524–6528.
10 C.-Y. Chiu, Y. Li, L. Ruan, X. Ye, C. B. Murray and Y. Huang, *Nature Chem.*, 2011, **3**, 393–399.
11 L. Ruan, H. Ramezani-Dakhel, C.-Y. Chiu, Y. Li, H. Heinz and Y. Huang, *Nano Lett.*, 2013, **13**, 840–846.
12 Y. Li, Z. Tang, P. N. Prasad, M. R. Knecht and M. T. Swihart, *Nanoscale*, 2014, **6**, 3165.
13 N. M. Bedford, H. Ramezani-Dakhel, J. M. Slocik, B. D. Briggs, Y. Ren, A. I. Frenkel, V. Petkov, H. Heinz, R. R. Naik and M. R. Knecht, *ACS Nano*, 2015, **9**, 5082–5092.
14 Z. Tang, C.-K. Lim, J. P. Palafox-Hernandez, K. L. M. Drew, Y. Li, M. T. Swihart, P. N. Prasad, T. R. Walsh and M. R. Knecht, *Nanoscale*, 2015, **7**, 13638–13645.
15 N. M. Bedford, Z. E. Hughes, Z. Tang, Y. Li, B. D. Briggs, Y. Ren, M .T. Swihart, V. G. Petkov, R. R. Naik, M. R. Knecht and T. R. Walsh, *J. Amer. Chem. Soc.*, 2016, **138**, 540-548.
16 J. Zeng, Y. Zheng, M. Rycenga, J. Tao, Z.-Y. Li, Q. Zhang, Y. Zhu and Y. Xia, *J. Amer. Chem. Soc.*, 2010, **132**, 8552–8553.
17 G. V. Hartland, *Chem. Rev.*, 2011, **111**, 3858–3887.
18 K. M. Mayer and J. H. Hafner, *Chem. Rev.*, 2011, **111**, 3828–3857.
19 J. L. C. Fajín, A. Bruix, M. N. D. S. Cordeiro, J. R. B. Gomes and F. Illas, *J. Chem. Phys.*, 2012, **137**, 034701.
20 M. Hu, D. P. Linder, M. Buongiorno Nardelli and A. Striolo, *J. Phys. Chem. C*, 2013, **117**, 15050–15060.
21 G. Frens, *Nature, Phys. Sci.*, 1973, **241**, 20–22.
22 R. P. Brinas, M. Maetani and J. J. J. Barchi, *J. Colloid Interface Sci.*, 2013, **392**, 415–421.
23 P. A. Mirau, R. R. Naik and P. Gehring, *J. Am. Chem. Soc.*, 2011, **133**, 18243–18248.
24 H. Heinz, B. L. Farmer, R. B. Pandey, J. M. Slocik, S. S. Patnaik, R. Pachter and R. R. Naik, *J. Am. Chem. Soc.*, 2009, **131**, 9704–9714.
25 R. Di Felice and S. Corni, *J. Phys. Chem. Lett*, 2011, **2**, 1510–1519.
26 A. Vila Verde, P. J. Beltramo and J. K. Maranas, *Langmuir*, 2011, **27**, 5918–5926.
27 J. Feng, J. M. Slocik, M. Sarikaya, R. R. Naik, B. L. Farmer and H. Heinz, *Small*, 2012, **8**, 1049–1059.
28 Z. Tang, J. P. Palafox-Hernandez, W.-C. Law, Z. E. Hughes, M. T. Swihart, P. N. Prasad, M. R. Knecht and T. R. Walsh, *ACS Nano*, 2013, **7**, 9632–9646.
29 G. Nawrocki and M. Cieplak, *J. Phys. Chem. C*, 2014, **118**, 12929–12943.
30 M. J. Penna, M. Mijajlovic and M. J. Biggs, *J. Am. Chem. Soc.*, 2014, **136**, 5323–5331.
31 L. Bellucci and S. Corni, *J. Phys. Chem. C*, 2014, **118**, 11357–11364.
32 Z. Tang, C. K. Lim, J. P. Palafox-Hernandez, Z. E. Hughes, Y. Li, M. T. Swihart, P. N. Prasad, T. R. Walsh and M. R. Knecht, *Chem. Mater.*, 2014, **26**, 4960–4969.
33 L. B. Wright, N. A. Merrill, M. R. Knecht and T. R. Walsh, *ACS Appl. Mater. Interfaces*, 2014, **6**, 10524–10533.
34 L. B. Wright, J. P. Palafox-Hernandez, P. M. Rodger, S. Corni and T. R. Walsh, *Chem. Sci.*, 2015, **6**, 5204–5214.

35 J. Yu, M. L. Becker and G. A. Carri, *Small*, 2010, **6**, 2242–2245.

36 L. B. Wright, P. M. Rodger, S. Corni and T. R. Walsh, *J. Chem. Theory Comput.*, 2013, **9**, 1616–1630.

37 L. B. Wright, P. M. Rodger, T. R. Walsh and S. Corni, *J. Phys. Chem. C*, 2013, **117**, 24292–24306.

38 Z. E. Hughes, L. B. Wright and T. R. Walsh, *Langmuir*, 2013, **29**, 13217–13229.

39 O. D. Häberlen, S.-C. Chung, M. Stener and N. Rösch, *J. Chem. Phys.*, 1997, **106**, 5189–5201.

40 39 E. Fernández, J. Soler and L. Balbás, *Phys. Rev. B*, 2006, **73**, 235433.

41 B. C. Curley, R. L. Johnston, N. P. Young, Z. Y. Li, M. DiVece, R. E. Palmer and A. L. Bleloch, *J. Phys. Chem. C*, 2007, **111**, 17846–17851.

42 A. Roldán, F. Viñes, F. Illas, J. M. Ricart and K. M. Neyman, *Theo. Chem. Acc.*, 2008, **120**, 565–573.

43 F. Viñes, F. Illas and K. M. Neyman, *J. Phys. Chem. A*, 2008, **112**, 8911–8915.

44 A. S. Barnard and L. A. Curtiss, *ChemPhysChem*, 2006, **7**, 1544–1553.

45 A. S. Barnard, *Acc. Chem. Res.*, 2012, **45**, 1688–1697.

46 W. Andreoni, A. Curioni and H. Grönbeck, *Int. J. Quant. Chem.*, 2000, **80**, 598–608.

47 D. Krüger, H. Fuchs, R. Rousseau, D. Marx and M. Parrinello, *J. Chem. Phys.*, 2001, **115**, 4776.

48 F. Viñes, Y. Lykhach, T. Staudt, M. P. A. Lorenz, C. Papp, H.-P. Steinrück, J. Libuda, K. M. Neyman and A. Görling, *Chem. Eur. J.*, 2010, **16**, 6530–6539.

49 A. S. Barnard, *Cryst. Growth Des.*, 2013, **13**, 5433–5441.

50 H.-T. Chen, J.-G. Chang, S.-P. Ju and H.-L. Chen, *J. Phys. Chem. Lett.*, 2010, **1**, 739–742.

51 G. Periyasamy, E. Durgun, J.-Y. Raty and F. Remacle, *J. Phys. Chem. C*, 2010, **114**, 15941–15950.

52 M. Askerka, D. Pichugina, N. Kuz'menko and A. Shestakov, *J. Phys. Chem. A*, 2012, **116**, 7686–7693.

53 J. A. Carr, H. Wang, A. Abraham, T. Gullion, J. P. Lewis, *J. Phys. Chem. C*, 2012, **116**, 25816–25823.

54 H. Barrón, L. Fernández-Seivane and X. López-Lozano, *Phys. Status Solid B*, 2014, **251**, 1239–1247.

55 Y. Wang, H. Su, C. Xu, G. Li, L. Gell, S. Lin, Z. Tang, H. Häkkinen and N. Zheng, *J. Am. Chem. Soc.*, 2015, **137**, 4324–4327.

56 P. Joshi, V. Shewale, R. Pandey, V. Shanker, S. Hussain and S. P. Karna, *J. Phys. Chem. C*, 2011, **115**, 22818–22826.

57 G. Brancolini, D. B. Kokh, L. Calzolai, R. C.Wade and S. Corni, *ACS Nano*, 2012, **6**, 9863–9878.

58 G. Peng and M. Mavrikakis, *Nano Lett.*, 2015, **15**, 629–634.

59 T. R. Walsh, *Phys. Chem. Chem. Phys*, 2005, **7**, 443–451.

60 K. Berland, V. R. Cooper, K. Lee, E. Schröder, T. Thonhauser, P. Hyldgaard and B. I. Lundqvist, *Rep. Prog. Phys.*, 2015, **78**, 066501.

61 H. Hu, L. Reven and A. Rey, *J. Phys. Chem. B*, 2013, **117**, 12625–12631.

62 J. Kleis, J. Greeley, N. A. Romero, V. A. Morozov, H. Falsig, A. H. Larsen, J. Lu, J. J. Mortensen, M. Dulak, K. S. Thygesen, J. K. Nørskov, and K. W. Jacobsen, *Catal. Lett.*, 2011, **141**, 1067-1071.

63 A. H. Larsen, J. Kleis, K. S. Thygesen, J. K. Nørskov and K. W. Jacobsen, *Phys. Rev. B.*, 2011, **84**, 245429.

64 M. Dion, H. Rydberg, E. Schröder, D. C. Langreth and B. I. Lundqvist, *Phys. Rev. Lett.*, 2004, **92**, 246401.

65 J. Klimeš and A. Michaelides, *J. Chem. Phys.*, 2012, **137**, 120901.

66 W. Liu, J. Carrasco, B. Santra, A. Michaelides, M. Scheffler and A. Tkatchenko, *Phys. Rev. B*, 2012, **86**, 245405.

67 W. Liu, V. G. Ruiz, G.-X. Zhang, B. Santra, X. Ren, M. Scheffler and A. Tkatchenko, *New J. Phys.*, 2013, **15**, 053046.

68 J. Carrasco, W. Liu, A. Michaelides and A. Tkatchenko, *J. Chem. Phys.*, 2014, **140**, 084704.

69 B. Liu, L. Cheng, L. Curtiss and J. Greeley, *Surf. Sci.*, 2015, **622**, 51–59.

70 R. Cortese, R. Schimmenti, N. Armata, F. Ferrante, A. Prestianni, D. Duca and D. Y. Murzin, *J. Phys. Chem. C*, 2015, **119**, 17182–17192.

71 J. Matos, H. Yildirim and A. Kara, *J. Phys. Chem. C*, 2015, **119**, 1886–1897.

72 P. Giannozzi et al., *J. Phys. Condens. Matter*, 2009, **21**, 395502.

73 Y. Zhang and W. Yang, *Phys. Rev. Lett.*, 1998, **80**, 890.

74 D. Vanderbilt, *Phys. Rev. B,* 1990, **41**, 7892.

75 J. Perdew, K. Burke and M. Ernzerhof, *Phys. Rev. Lett.*, 1996, **77**, 3865–3868.

76 J. P. Perdew, A. Ruzsinszky, G. I. Csonka, O. A. Vydrov, G. E. Scuseria, L. A. Constantin, X. Zhou and K. Burke, *Phys. Rev. Lett.*, 2008, **100**, 136406.

77 F. Iori, R. Di Felice, E. Molinari and S. Corni, *J. Comput. Chem.*, 2009, **30**, 1465–1476.

78 A. A. Skelton, T. N. Liang and T. R. Walsh, *ACS Appl. Mater. Interfaces,* 2009, **1**, 1482–1491.

79 76 J. Schneider and L. Colombi Ciacchi, *J. Am. Chem. Soc.*, 2012, **134**, 2407–2413.

80 H. Heinz, R. A. Vaia, B. L. Farmer and R. R. Naik, *J. Phys. Chem. C*, 2008, **112**, 17281.

81 J. Carrasco, A. Hodgson and A. Michaelides, *Nat. Mater.*, 2012, **11**, 667-674.

82 J. Carrasco, J. Klimeš and A. Michaelides, *J. Chem. Phys.*, 2013, **138**, 024708.

83 T. J. Lawton, J. Carrasco, A. E. Baber, A. Michaelides, and E. C. H. Sykes, *Phys. Rev. Lett.*, 2011, **107**, 256101.

84 E. M. Karp, T. L. Silbaugh, M. C. Crowe, and C T. Campbell, *J. Am. Chem. Soc.*, 2012, **134**, 20388–20395.

85 C. J. Murphy, J. Carrasco, T. J. Lawton, M. L. Liriano, A. E. Baber, E. A. Lewis, A. Michaelides, and E. C. H. Sykes, *J. Chem. Phys.*, 2014, **141**, 014701.

86 H. Yildirim, T. Greber and A. Kara, *J. Phys. Chem. C*, 2013, **117**, 20572-20583.

87 Z. E. Hughes and T. R. Walsh, *J. Colloid Interface Sci.*, 2014, **436**, 99-110.